ChemComm

COMMUNICATION

View Article Online
View Journal | View Issue

Cite this: *Chem. Commun.*, 2024, **60**, 1472

Received 16th November 2023,
Accepted 12th December 2023

DOI: 10.1039/d3cc05628g

rsc.li/chemcomm

A reductively convertible nickel phthalocyanine precursor as a biological thiol-responsive turn-on photoacoustic contrast agent†

Kohei Nogita,[a] Takaya Sugahara,[a] Koji Miki, *[a] Huiying Mu,[a] Minoru Kobayashi,[b] Hiroshi Harada[b] and Kouichi Ohe *[a]

A nickel phthalocyanine precursor bearing poly(ethylene glycol) as a turn-on contrast agent for photoacoustic imaging was prepared. The water-soluble polymeric chains were smoothly eliminated through thiol-mediated reductive aromatization in cancer cells, enabling the detection of endogenous biological thiols *in vitro* and *in vivo*.

Photoacoustic (PA) imaging has attracted attention as a reliable method to visualize cancer tissues *in vivo* because of its advantages, such as high spatial resolution, deeper tissue visualization, and low invasiveness.[1] Metallophthalocyanine (MPc) is a photostable near-infrared (NIR)-absorbing dye and is considered one of the most promising photosensitizers for PA imaging because of its high molar extinction coefficient and excellent photothermal conversion efficiency.[2] Although MPc-containing nanoparticles[3] and water-soluble MPcs[4] have been used for PA cancer imaging, they generate PA signals as background noise in normal tissues. Several 'activatable' contrast agents based on MPc, which can enhance PA signal intensity in response to tumour-specific biological compounds, have been developed to visualize cancer tissue more clearly.[5] Despite the activatable nature of such MPc agents, generating background PA signals by unreacted MPcs still needs to be suppressed for efficient imaging with high contrast. Therefore, a 'turn-on' PA photosensitizer that generates PA signals only in cancer tissues is ideal;[6] however, to our knowledge, there is no example of a turn-on PA contrast agent based on MPc. Modified MPcs with two alkoxy substituents at the α-position of pyrroles (ox-MPc) were reported as thermally convertible MPc precursors (Fig. 1a).[7] Considering that the transformation of ox-MPc to MPc is a formal reduction reaction, reductive aromatization is a more suitable conversion method.[8] We envisioned that biological thiols such as glutathione (GSH) overexpressed in many cancer cell lines can be utilized for the reductive aromatization of ox-MPcs under physiological conditions.[9]

Herein, we report the turn-on PA contrast agent **ox-NiPc-PEG** consisting of ox-NiPc and water-soluble poly(ethylene glycol) (PEG) (Fig. 1b). Because the introduction of two alkoxy groups on the 18π aromatic core structure of NiPc causes a hypsochromic shift in the absorption peak of **ox-NiPc-PEG**, no PA signal is generated under NIR pulsed laser irradiation for PA imaging. The conversion of **ox-NiPc-PEG** to NiPc by GSH proceeded under physiological conditions, resulting in strong PA signal

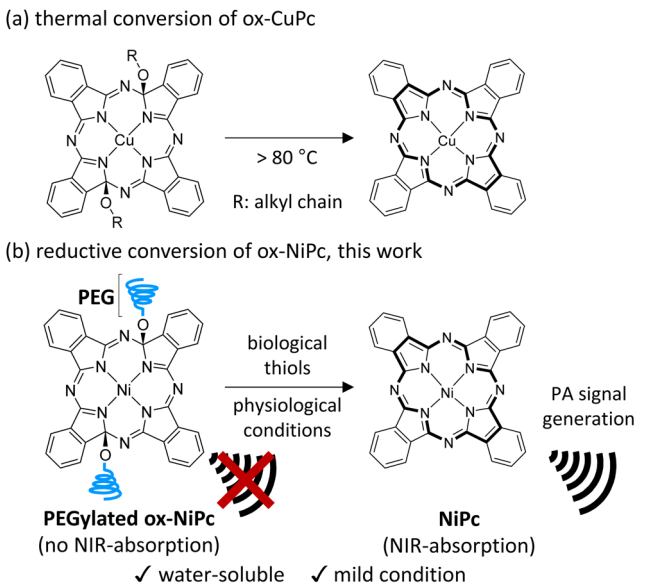

Fig. 1 (a) Thermal conversion of ox-CuPc and (b) reductive-conversion of ox-NiPc.

[a] *Department of Energy and Hydrocarbon Chemistry, Graduate School of Engineering, Kyoto University, Katsura, Nishikyo-ku, Kyoto 615-8510, Japan. E-mail: kojimiki@scl.kyoto-u.ac.jp, ohe@scl.kyoto-u.ac.jp*

[b] *Laboratory of Cancer Cell Biology, Graduate School of Biostudies, Kyoto University, Yoshida Konoe-cho, Sakyo-ku, Kyoto 606-8501, Japan*

† Electronic supplementary information (ESI) available: Experimental section, MTT assay, spectroscopic, and NMR spectra. CCDC 2303413. For ESI and crystallographic data in CIF or other electronic format see DOI: https://doi.org/10.1039/d3cc05628g

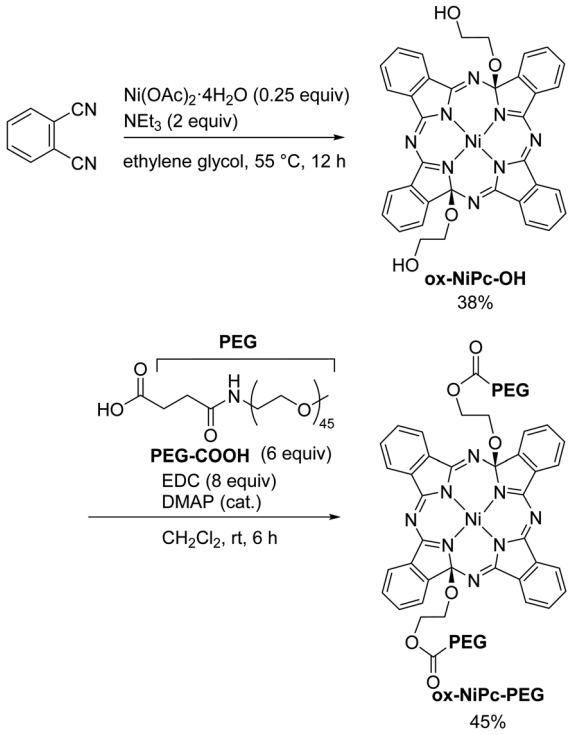

Scheme 1 Synthesis of **ox-NiPc-PEG**.

generation. PA imaging using **ox-NiPc-PEG** enabled the detection of GSH in xenograft tumour-bearing mice.

The water-soluble NiPc precursor **ox-NiPc-PEG** was synthesized from phthalonitrile in two steps *via* **ox-NiPc-OH** with two hydroxy groups at the side chain terminal (Scheme 1). The structure of **ox-NiPc-OH** was confirmed by X-ray crystallographic analysis (Fig. 2). The crystal structure clarified that two hydroxyethoxy groups on the α-carbons of diagonal pyrrole extended to the convex face of the significantly distorted NiPc macrocycle having sp^3-hybridized carbons.[7,10] The formation of the thermodynamically less stable *trans*-isomer was not observed (Fig. S4 and Table S1, ESI†). **ox-NiPc-OH** with a distorted structure could dissolve well in common organic solvents, such as toluene, THF, acetone, CH_2Cl_2, and $CHCl_3$. To enhance the water solubility of ox-NiPc, **ox-NiPc-PEG** was synthesized from **ox-NiPc-OH** by condensation with PEG derivative **PEG-COOH**[11] in 45% yield. **ox-NiPc-PEG** dissolved in water at the concentration of 500 μM or below (Fig. S3, ESI†).

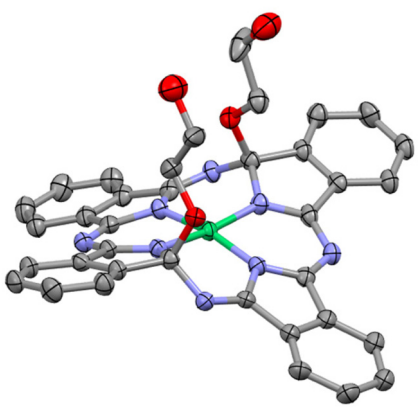

Fig. 2 ORTEP drawing of **ox-NiPc-OH** (50% ellipsoids). Hydrogen atoms and solvent molecules are omitted for clarity.

Next, we examined the reactivity of ox-NiPcs with reductants. The reaction of **ox-NiPc-PEG** with GSH in phosphate buffer solution (PBS) at room temperature gave a blue solid. This solid was identified as NiPc by MALDI-TOF mass spectrometry, IR absorption spectrometry, and elemental analysis (Fig. S5, S6 and Table S2, ESI†). When **ox-NiPc-OH** was treated with GSH at room temperature for 24 h, NiPc was obtained in 98% isolated yield. The UV-vis absorption spectrum of an aqueous solution of **ox-NiPc-PEG** showed no absorption signals in the NIR region because of the non-aromatic nature of the distorted NiPc core (Fig. 3a, red line). After the reaction of **ox-NiPc-PEG** with GSH in aqueous solution, a new absorption peak at 606 nm appeared (Fig. 3a, blue line). The absorption of the Q band of NiPc, which is generally observed at approximately 670 nm, was broadened and blue-shifted, indicating that NiPc formed *H*-aggregates in water.[12] These results showed that ox-NiPc can be quantitatively transformed to NiPc by reduction and utilized as a biological thiol-responsive photosensitizing molecule under physiological conditions.

Next, we examined the dependency of pH on the GSH-mediated reduction of **ox-NiPc-PEG**. The conversion of **ox-NiPc-PEG** to NiPc was accelerated in acidic PBS, and the resulting NiPc aggregates generated strong PA signals under NIR pulsed laser irradiation (Fig. 3b). This result suggests that the protonation of the alkoxy groups attached to pyrrole α-carbons is crucial in the reductive aromatization of **ox-NiPc-PEG**.[8] A plausible reaction mechanism is shown in Fig. 3c. Upon protonation, the alcohol is eliminated by a nucleophilic attack of biological thiols on the sp^3-hybridized carbon. The subsequent nucleophilic attack of biological thiol to thioether affords an 18π aromatic structure of the NiPc core together with a disulfide and alcohols.

To evaluate the GSH-mediated turn-on of the PA signal, we investigated the increase in the PA signal intensity of **ox-NiPc-PEG** under various GSH concentrations (Fig. 4a). The PA signal intensity was dependent on the GSH concentration. By contrast, the PA signal intensity of **ox-NiPc-PEG** scarcely increased in the absence of GSH. When **ox-NiPc-PEG** was treated with GSH at the intracellular concentrations, the PA signal intensity was 4.9- and 6.3-fold higher than when treated with Cys and Hcy, respectively (Fig. 4b). These results indicate that NiPc was produced more effectively upon treatment with GSH at the intracellular concentration. We confirmed that no $^1O_2$ was generated from NiPc, which is produced from **ox-NiPc-PEG** under NIR photoirradiation.[12] Therefore, the oxidative stress to normal cells by $^1O_2$ is expected to be avoidable during PA imaging using the NiPc precursor (Fig. S7, ESI†).

Having confirmed that the reduction of **ox-NiPc-PEG** can be monitored by the PA signal output, we next evaluated the PA signal intensity of **ox-NiPc-PEG** in GSH-overexpressing human lung cancer cell line A549.[13] After incubation with **ox-NiPc-PEG**

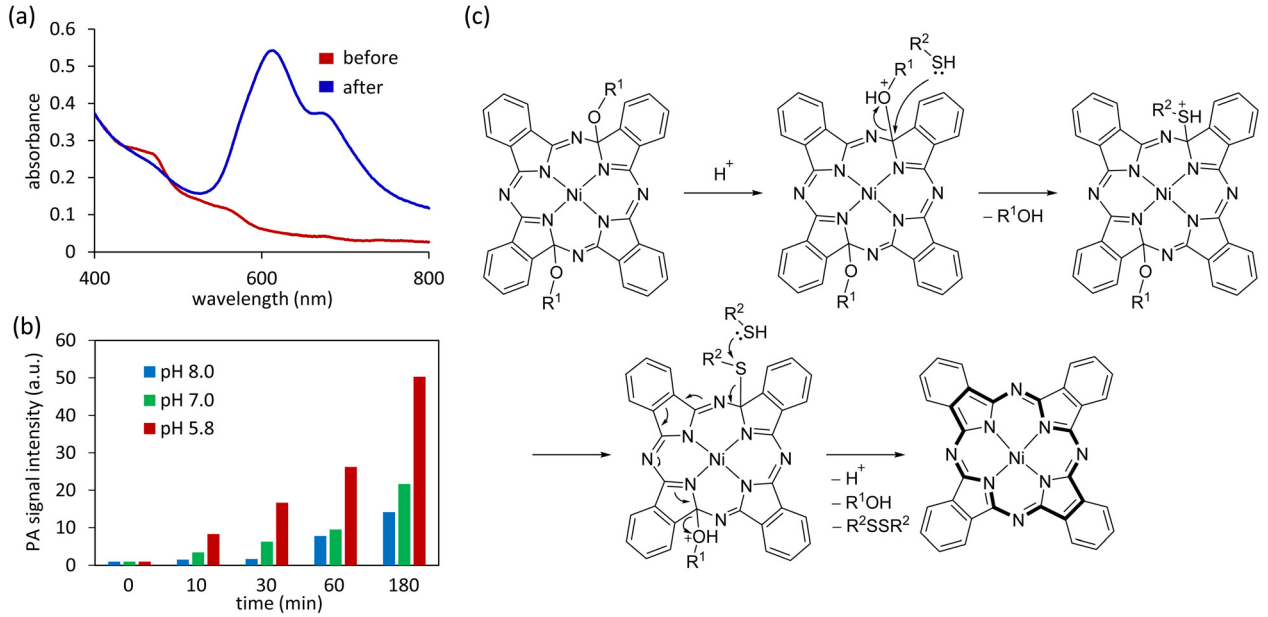

Fig. 3 (a) UV-vis absorption spectra of **ox-NiPc-PEG** (50 μM) in water before (red line) and after (blue line) GSH treatment. (b) Time-dependent PA signal intensity change of **ox-NiPc-PEG** in PBS at various pH (blue: pH 8.0, green: pH 7.0, red: pH 5.8) under GSH treatment (1 mM). Excitation wavelength is 680 nm. (c) Plausible mechanism of biological thiol-mediated reductive aromatization.

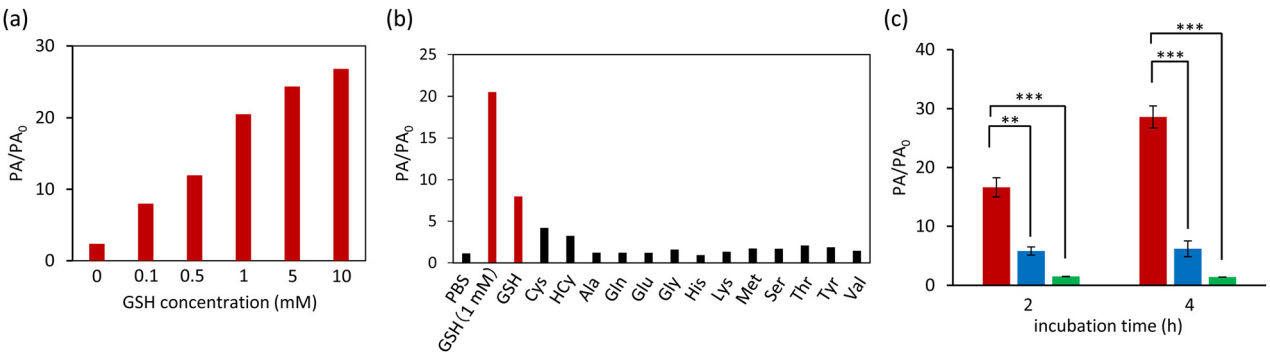

Fig. 4 (a) GSH concentration-dependent PA signal intensity of **ox-NiPc-PEG** (0.25 mM) in PBS (pH = 5.8) after 30 min. (b) PA signal intensity of **ox-NiPc-PEG** after incubation with GSH (1.0 mM or 0.10 mM, red) or amino acids (0.10 mM, black) in PBS (pH = 5.8) for 1 h at 37 °C. (c) Time-dependent PA signal intensity change during the incubation of A549 (red) and HEK293 (blue) with **ox-NiPc-PEG** (10 μM), and the incubation of A549 with **ox-NiPc-PEG** (10 μM) after incubation with NEM (green). Excitation wavelength is 680 nm. Two-tailed Student's *t*-test: $^{**}p < 0.01$, $^{***}p < 0.001$.

(10 μM), the PA signal intensity was significantly increased in A549 cells. After 4 h, the PA signal intensity in A549 cells was 4.6-fold stronger than that in the normal cell line HEK293 (Fig. 4c, red and blue). By a control experiment using *N*-ethylmaleimide (NEM) as a trapping agent of biological thiols in A549 cells, we confirmed that the increase in PA signal intensity was due to the formation of NiPc (Fig. 4c, green). It was confirmed that there was no cytotoxicity of **ox-NiPc-PEG** for cancer cells and normal cells when the concentration of **ox-NiPc-PEG** was less than 50 μM, using an MTT assay (Fig. S8, ESI†). These results indicate that **ox-NiPc-PEG** is suitable for use as a PA contrast agent to visualize the reductive environment of the tumour site *in vivo*.

Finally, we conducted PA imaging in living mice to verify the applicability of **ox-NiPc-PEG** as a biological thiol-responsive PA contrast agent *in vivo* (Fig. S9, ESI†). A549 cells were xenografted into the right legs of nude mice to prepare tumour-bearing mice. Eight prepared mice were divided into two groups for *in vivo* experiments through intratumoral administration. For the first group, saline (30 mL) was pre-treated at the tumour site in the right leg and the normal muscle in the left leg. After 30 min pre-treatment, **ox-NiPc-PEG** was administered intratumorally in the right leg and subcutaneously in the left leg, respectively. For the second group, a pre-treatment of NEM (2.0 mM in 30 μL saline) was conducted in tumour sites before the intratumoral administration of **ox-NiPc-PEG**. The PA tomography system was used to obtain horizontal and vertical view images at the indicated time points of post-injection of **ox-NiPc-PEG** (Fig. 5a), and the PA signal intensities at the administration sites were evaluated under NIR pulsed laser irradiation (Fig. 5b and Fig. S10–S12,

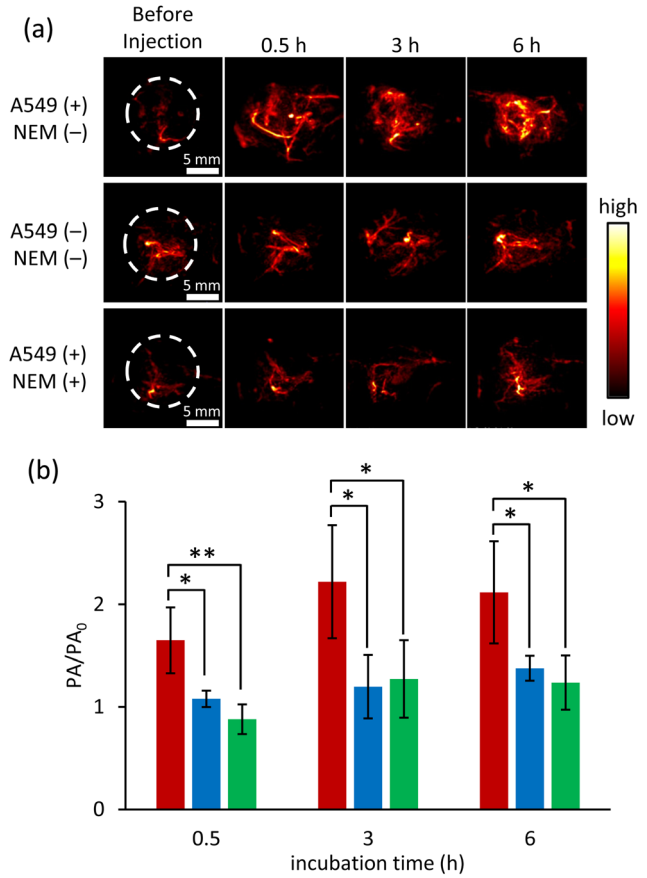

Fig. 5 (a) *In vivo* PA top-view images of administrated sites before and 0.5, 3, 6 hours after injection. (A549(+): tumor site, A549(−): normal muscle) (b) normalized PA signal intensity at the tumor sites (red: NEM(−), green: NEM(+)) and normal muscle (blue) at 0.5, 3, 6 h after intratumoral or subcutaneously injection of **ox-NiPc-PEG** (sample size: n = 4). Excitation wavelength is 680 nm. Two-tailed Student's t-test: *$p < 0.05$, **$p < 0.01$.

ESI†). After the injection of **ox-NiPc-PEG**, PA signal intensity in the tumour site significantly increased in three hours ($p < 0.05$) in good contrast to the non-tumour site, demonstrating its sensitivity to distinguish tumour sites from normal muscle. Furthermore, the NEM-pretreated tumours exhibited weak PA signals before and after injection, suggesting that **ox-NiPc-PEG** can selectively detect biological thiols in living mice.

In conclusion, we have developed a turn-on PA contrast agent based on reductive aromatization for cancer imaging. A water-soluble NiPc precursor **ox-NiPc-PEG** was converted to NiPc by biological thiols, generating strong PA signals under NIR pulsed laser irradiation. Because the biological thiol-mediated transformation proceeded smoothly under acidic conditions, the protonation of the alkoxy groups was considered to be crucial in the reductive aromatization. The results obtained *in vitro* and *in vivo* demonstrated that the increase in PA signal intensity was mainly due to the reduction of **ox-NiPc-PEG** by GSH overexpressed in cancer cells. Because biological thiol-mediated reductive aromatization proceeds under mild physiological conditions, it is suitable for constructing a π-conjugated system of photosensitizer *in vivo*.

This work was supported by JST, the establishment of university fellowships towards the creation of science technology innovation, Grant Number JPMJFS2123. K. M. appreciates the financial supports from The Asahi Glass Foundation and The Uehara Memorial Foundation. We acknowledged Prof. Teruyuki Kondo and Associate Prof. Yu Kimura in Kyoto University for PA imaging. A part of this study was conducted through the CORE Program of the Radiation Biology Center, Kyoto University.

Conflicts of interest

There are no conflicts to declare.

Notes and references

1 (*a*) J. Weber, P. C. Beard and S. E. Bohndiek, *Nat. Methods*, 2016, **16**, 639–650; (*b*) R. E. Borg and J. Rochford, *Photochem. Photobiol.*, 2018, **94**, 1175–1209; (*c*) W. Choi, B. Park, S. Choi, D. Oh, J. Kim and C. Kim, *Chem. Rev.*, 2023, **123**, 7379–7419.
2 (*a*) E.-Y. Park, D. Oh, S. Park, W. Kim and C. Kim, *APL Bioeng.*, 2021, **5**, 031510; (*b*) D. Li, S. Cai, P. Wang, H. Cheng, B. Cheng, Y. Zhang and G. Liu, *Adv. Healthcare Mater.*, 2023, 2300263; (*c*) B.-D. Zheng, J. Ye, Y.-Y. Huang and M. T. Xiao, *Biomater. Sci.*, 2021, **9**, 7811–7825.
3 (*a*) K. Strokov, A. H. Schäfer, U. Dobrindt and A. Galstyan, *ACS Appl. Bio Mater.*, 2020, **3**, 3751–3760; (*b*) X. Li, S. Yu, Y. Lee, T. Guo, N. Kwon, D. Lee, S. C. Yeom, Y. Cho, G. Kim, J.-D. Huang, S. Choi, K. T. Nam and J. Yoon, *J. Am. Chem. Soc.*, 2019, **141**, 1366–1372; (*c*) A. Shaukat, E. Anaya-Plaza, S. Julin, V. Linko, T. Torres, A. de la Escosura and M. A. Kostiainen, *Chem. Commun.*, 2020, **56**, 7341–7344.
4 (*a*) X. Li, E.-Y. Park, Y. Kang, N. Kwon, M. Yang, S. Lee, W. J. Kim, C. Kim and J. Yoon, *Angew. Chem., Int. Ed.*, 2020, **59**, 8630–8634; (*b*) S. Li, L. Zhao, R. Chang, R. Xing and X. Yan, *Chem. – Eur. J.*, 2019, **25**, 13429–13435; (*c*) X. Li, C. Kim, S. Lee, D. Lee, H.-M. Chung, G. Kim, S.-H. Heo, C. Kim, K.-S. Hong and J. Yoon, *J. Am. Chem. Soc.*, 2017, **139**, 10880–10886.
5 (*a*) C. Xie, X. Zhen, Y. Lyu and K. Pu, *Adv. Mater.*, 2017, **29**, 1703693; (*b*) K. Nogita, K. Miki, N. Imaizumi, M. Oe, H. Mu and K. Ohe, *J. Photochem. Photobiol., A*, 2023, **438**, 114547; (*c*) K. Miki, N. Imaizumi, K. Nogita, M. Oe, H. Mu, W. Huo, H. Harada and K. Ohe, *Bioconjugate Chem.*, 2021, **32**, 1773–1781.
6 (*a*) Z. Zhao, C. B. Swartchick and J. Chan, *Chem. Soc. Rev.*, 2022, **51**, 829–868; (*b*) J. Huang and K. Pu, *Angew. Chem., Int. Ed.*, 2020, **59**, 11717–11731; (*c*) Y. Liu, L. Teng, B. Yin, H. Meng, X. Yin, S. Huan, G. Song and X.-B. Zhang, *Chem. Rev.*, 2022, **122**, 6850–6918; (*d*) Y. Zeng, T. Dou, L. Ma and J. Ma, *Adv. Sci.*, 2022, **9**, 2202384.
7 (*a*) Y. Kikukawa, T. Fukuda, A. Fuyuhiro, N. Ishikawa and N. Kobayashi, *Chem. Commun.*, 2011, **47**, 8518–8520; (*b*) T. Fukuda, Y. Kikukawa, R. Tsuruya, A. Fuyuhiro, N. Ishikawa and N. Kobayashi, *Inorg. Chem.*, 2011, **50**, 11832–11837; (*c*) T. Fukuda and N. Ishikawa, *Dyes Pigm.*, 2014, **109**, 151–154.
8 J. L. Marshall, D. Lehnherr, B. D. Lindner and R. R. Tykwinski, *ChemPlusChem*, 2017, **82**, 967–1001.
9 (*a*) R. Kaushik, N. Nehra, V. Novakova and P. Zimcik, *ACS Omega*, 2023, **8**, 98–126; (*b*) W. Xie, J. Jiang, D. Shu, Y. Zhang, S. Yang and K. Zhang, *Molcules*, 2023, **28**, 4252; (*c*) J. Dai, C. Ma, P. Zhang, Y. Fu and B. Shen, *Dyes Pigm.*, 2020, **177**, 108321; (*d*) H. S. Jung, X. Chen, K. Seung and J. Yoon, *Chem. Soc. Rev.*, 2013, **42**, 6019–6031; (*e*) P. Anees, J. Joseph, S. Sreejith, N. V. Menon, Y. Kang, S. W.-K. Yu, A. Ajayaghosh and Y. Zhao, *Chem. Sci.*, 2016, **7**, 4110–4116; (*f*) H. Mu, K. Miki, T. Kubo, K. Otsuka and K. Ohe, *Chem. Commun.*, 2021, **57**, 1818–1821.
10 (*a*) C. D. Molek, J. A. Halfen, J. C. Loe and R. W. McGaff, *Chem. Commun.*, 2001, 2644–2645; (*b*) Y. Y. Karabach, M. N. Kopylovich, K. V. Luzyanin, M. F. C. Guedes da Silva, V. Yu. Kukushkin and A. J. L. Pombeiro, *Inorg. Chem. Acta*, 2017, **455**, 696–700.
11 M. E. Ourailidou, P. Dockerty, M. Witte, G. J. Poelarends and F. J. Dekker, *Org. Biomol. Chem.*, 2015, **13**, 3648–3653.
12 No generation of $^1O_2$ from NiPc was reported. See: G. F. M. Pereira and T. T. Tasso, *Inorg. Chim. Acta*, 2021, **519**, 120271.
13 K. Umezawa, M. Yoshida, M. Kamiya, T. Yamasoba and Y. Urano, *Nat. Chem.*, 2017, **9**, 279–286.